6-8-2024

Development of primary osteoarthritis during aging in genetically diverse UM-HET3 mice.

Sher Bahadur Poudel

Ryan R Ruff

Gozde Yildirim

Richard A Miller

David E Harrison

See next page for additional authors

Authors

Sher Bahadur Poudel, Ryan R Ruff, Gozde Yildirim, Richard A Miller, David E Harrison, Randy Strong, Thorsten Kirsch, and Shoshana Yakar

Development of primary osteoarthritis during aging in genetically diverse UM-HET3 mice

Sher Bahadur Poudel[1], Ryan R. Ruff[2], Gozde Yildirim[1], Richard A. Miller[3], David E. Harrison[4], Randy Strong[5,6], Thorsten Kirsch[7,8] and Shoshana Yakar[1]*

Abstract

Background Primary osteoarthritis (OA) occurs without identifiable underlying causes such as previous injuries or specific medical conditions. Age is a major contributing factor to OA, and as one ages, various joint tissues undergo gradual change, including degeneration of the articular cartilage, alterations in subchondral bone (SCB) morphology, and inflammation of the synovium.

Methods We investigated the prevalence of primary OA in aged, genetically diverse UM-HET3 mice. Articular cartilage (AC) integrity and SCB morphology were assessed in 182 knee joints of 22-25 months old mice using the Osteoarthritis Research Society International (OARSI) scoring system and micro-CT, respectively. Additionally, we explored the effects of methylene blue (MB) and mitoquinone (MitoQ), two agents that affect mitochondrial function, on the prevalence and progression of OA during aging.

Results Aged UM-HET3 mice showed a high prevalence of primary OA in both sexes. Significant positive correlations were found between cumulative AC (cAC) scores and synovitis in both sexes, and osteophyte formation in female mice. Ectopic chondrogenesis did not show significant correlations with cAC scores. Significant direct correlations were found between AC scores and inflammatory markers in chondrocytes, including matrix metalloproteinase-13, inducible nitric oxide synthase, and the NLR family pyrin domain containing-3 inflammasome in both sexes, indicating a link between OA severity and inflammation. Additionally, markers of cell cycle arrest, such as p16 and β-galactosidase, also correlated with AC scores. In male mice, no significant correlations were found between SCB morphology traits and cAC scores, while in female mice, significant correlations were found between cAC scores and tibial SCB plate bone mineral density. Notably, MB and MitoQ treatments influenced the disease's progression in a sex-specific manner. MB treatment significantly reduced cAC scores at the medial knee joint, while MitoQ treatment reduced cAC scores, but these did not reach significance.

Conclusions Our study provides comprehensive insights into the prevalence and progression of primary OA in aged UM-HET3 mice, highlighting the sex-specific effects of MB and MitoQ treatments. The correlations between AC scores and various pathological factors underscore the multifaceted nature of OA and its association with inflammation and subchondral bone changes.

Keywords Osteoarthritis, UM-HET3, Sub-chondral bone, Cartilage, Methylene blue, Mitoquinone, Antioxidants

*Correspondence:
Shoshana Yakar
sy1007@nyu.edu
Full list of author information is available at the end of the article

Poudel *et al. Arthritis Research & Therapy*   (2024) 26:118

Page 2 of 14

Introduction

Primary osteoarthritis (OA) refers to the development of OA without any known underlying factors, conditions, or injuries. Aging is a significant risk factor for OA, and during the aging process, there are progressive changes in joint tissues, including articular cartilage, subchondral bone, synovium, and ligaments. These changes involve increased matrix degradation, altered cell metabolism, impaired tissue repair mechanisms [1], and chronic low-grade inflammation [2–5]. In knee OA, which is commonly associated with aging, the articular cartilage gradually deteriorates, becoming thinner and exhibiting structural abnormalities. This compromises its ability to absorb shock and distribute load, resulting in joint pain and dysfunction. The subchondral bone also undergoes remodeling, including thickening and sclerosis, contributing to joint stiffness and further impacting cartilage health. Inflammation in the synovial membrane increases, leading to the production of inflammatory mediators that contribute to cartilage degradation and joint inflammation [6].

Our understanding of primary OA is derived from both clinical and preclinical research. In vivo preclinical animal models that focus mainly on genetic- or injury-induced OA have been particularly useful for two key purposes: investigating the underlying mechanisms of OA and evaluating the effectiveness of various treatment options. However, clinical studies of primary OA have shown variability in the actual onset of the disease, in the rate of OA progression, and in the severity of OA in different individuals. Thus, while inbred mouse models have provided valuable insights into OA mechanisms, they lack the genetic complexity of the human population [7, 8], and provide only limited insights into the natural development of the disease. Studying OA using a single genome compromises generalization and translation of findings [9]. The UM-HET3 mouse model, generated through a specific crossbreeding strategy (Fig. 1A), offers a genetically heterogeneous population that better represents genetic diversity. The *UM-HET3 mouse model was selected by the Intervention Testing Program (ITP) at the National Institute of Aging (NIA) for studies of anti-aging drugs and was used in several studies to map genes controlling skeletal morphology* [10–13] (https://phenome.jax.org/projects/ITP1). A previous study has shown that UM-HET3 male mice (from one ITP center) developed age-related OA, but exhibited a high degree of variability, showing no significant effects of the tested ITP treatments [14]. In the current study we used 182 stifles of UM-HET3 mice from three ITP centers and explored both sexes.

Since OA occurrence intensifies with age, evaluating the presence and severity of OA becomes a crucial factor in assessing the effectiveness of compounds designed to prolong life by influencing pathways that might also play a role in OA development. Therefore, this study aimed to assess the severity of OA associated with aging in genetically diverse male and female mice and to investigate whether the severity of this age-related OA was altered in mice treated with specific agents from the ITP study. Specifically, since common cellular processes are shared between OA and aging, such as mitochondrial dysfunction, oxidative stress, increased inflammation, and accumulation of senescent cells [18], we focused on two compounds that enhance mitochondrial function. Mitochondrial dysfunction and imbalanced production of reactive oxygen species (ROS) are considered contributing factors to OA development [19–21]. Impaired mitochondrial function in chondrocytes is linked to various cellular mechanisms involved in energy regulation, inflammation, and pro-catabolic responses [22].

Two compounds that affect mitochondrial function were tested by the ITP centers, methylene blue (MB) and mitoquinone (MitoQ). Neither MB nor MitoQ altered lifespan in UM-HET3 mice [23]. MB, an FDA-approved drug used to treat methemoglobinemia, has been shown to enhance mitochondrial function and has demonstrated beneficial effects in animal models of OA [24]. Intra-articular injection of MB in rat and rabbit OA models improved joint symptoms, protected cartilage, and reduced inflammation [25] [26]. MitoQ, a mitochondria-targeted antioxidant [27–29], also suppressed ROS production and ATP synthesis in an osteochondral explant model [30] .Here we report the prevalence of primary OA and the effects of lifelong mitochondrial function enhancement on knee joint tissues during aging in the UM-HET3 mice [31].

Methods

Animals

UM-HET3 male and female mice were produced by a cross between (BALB/cByJ × C57BL/6J)F1 mothers (JAX stock #100009) and (C3H/HeJ × DBA/2J)F1 fathers (JAX stock #100004). Detailed housing conditions were specified elsewhere [32]. All the ITP sites used the same supplier of bedding and food was prepared centrally and shipped simultaneously to all sites (https://www.nia.nih.gov/research/dab/interventions-testing-program-itp). The mice were housed in plastic cages with metal covers and furnished with corn-cob bedding under similar environmental conditions in all sites (21-23°C temperature, 40-60% humidity and 12-hour light/dark cycle). Cages were adequately ventilated, and the mice were relocated to new cages at least every 7 days. Male mice were accommodated in groups of three per cage, while female mice were housed in
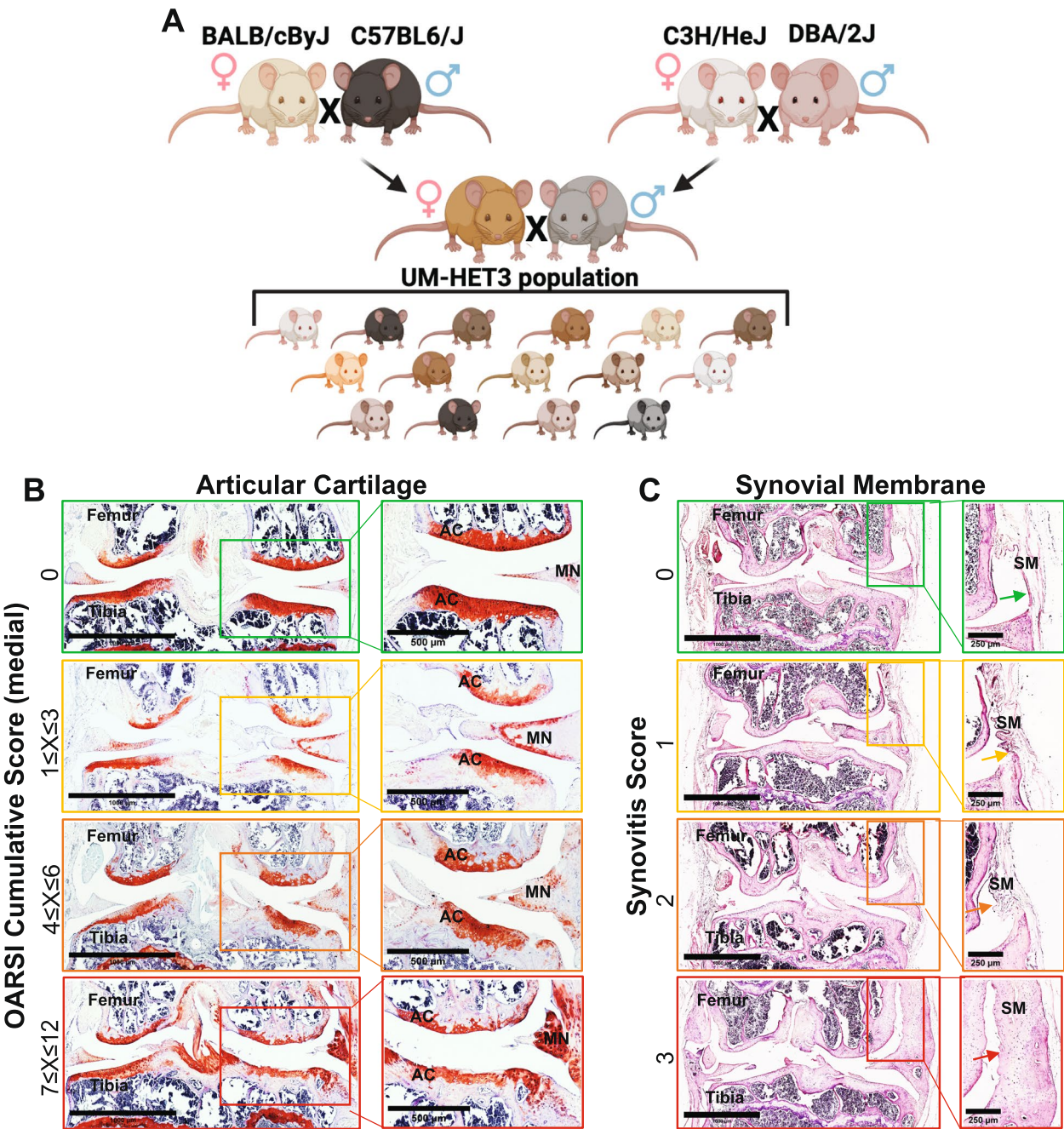
Fig. 1 OARSI scoring of stifles from UMHET3 mouse model. **A** UM-HET3 is a genetically diverse mouse model, generated via 4way cross of (BALB/ cByJ × C57BL/6J) F1 mothers and (C3H/HeJ × DBA/2J) F1 fathers. Each of the offspring is genetically unique but shares 50% of its genetic material with every other UM-HET3 mouse. **B** Shown are representative knee joint samples that were processed for safranin-O-red, or (C) H&E staining of the synovial membrane that were categorized based on the OARSI scoring system [15–17]

groups of four per cage. Mice had unrestricted access to water and food. Mice were euthanized by controlled CO_2 inflow to a chamber. Whole body was fixed and preserved in 4% formaldehyde solution prepared in 1X phosphate-buffered saline at 4^0C. Specific pathogen free status was quarterly assessed in each site. All experiments were approved by the Institutional Animal Care and Use Committee (IACUC) of each site (The Jackson Laboratory in Bar Harbor, Maine (TJL), the University of Michigan at Ann Arbor (UM), and the University of Texas Health Science Center at San Antonio (UT).

Poudel *et al. Arthritis Research & Therapy* (2024) 26:118

Page 4 of 14

Interventions (diets): Pharmacological grade MB and MitoQ were mixed in irradiated Purina test Diet 5LG6 at a concentration of 28 mg kg−1 (28 ppm) and 100 mg kg−1 (100 ppm) of diet respectively [23, 33]. The same batch of food was supplied to all the sites. The mice were fed MB containing food from 4 months and MitoQ from 7 months of age [23].

Micro computed tomography (micro-CT)

Right hind limbs were dissected (*n*=182, male control=47, female control=45, male MB=22, female MB=24, male MitoQ=22 and female MitoQ=22). Legs were washed three times in 1X PBS and proceed to Micro-CT in accordance to the American Society for Bone and Mineral Research (ASBMR) guidelines [34]. Intact femur and tibia including the knee joint were scanned using a high-resolution SkyScan micro-CT system (SkyScan 1172, Kontich, Belgium) containing 10-M digital detector set at a 10W energy level (100kV and 100 μA), with a 0.5 mm aluminum filter with a 9.7μm image voxel size. Subchondral bone (SCB) parameters were taken in the distal femur below the articular cartilage (AC) avoiding cortical bone and included bone volume fraction (bone volume/tissue volume, (BV/TV %), trabecular thickness (Tb.Th, mm), trabecular number (Tb.N, 1/mm), and bone mineral density (BMD, g/cc). Subchondral bone plate (SCBP) thickness and BMD were measured at the proximal tibia. Data reconstruction was done using NRecon software, and data analysis using CTAn software. 3D images were obtained using CT Vox software.

Histology

Following micro-CT scanning, intact hindlimbs were decalcified in 10% EDTA for 3-4 weeks. Decalcification was stopped when the bones were found soft and confirmed in random samples by x-ray. Decalcified samples were thoroughly washed in running tap water, dehydrated using graded alcohol series and xylene, and processed for paraffin embedding and sectioning. Samples were sectioned in a coronal plane to 5-μm sections. Sections from the mid coronal region were used for histological analyses. Safranin-O-red staining was used for scoring the AC of the knee joint, including the presence and maturation stage of osteophytes as well as the ectopic chodrogenesis and ossification. H&E staining was used to score inflammation of synovial membrane, and overall morphology. For all the scoring systems, six typical mid coronal sections covering approximately 80-μm were chosen, subjected to staining, and the mean score of sections were taken for calculations.

Osteoarthritis score

Cartilage damage at medial and lateral tibio-femoral joints was evaluated by two blinded observers using the Osteoarthritis Research Society International (OARSI) scoring system [15]. The cartilage damage quantification by safranin-O-red consisted 0, 0.5, 1-6 scores; Osteophyte maturity was scored 0, 1-4 according to previously described method [16], where 0 as no osteophyte detected; 1 when osteophytes were composed of precartilaginous lesion; 2 when osteophytes were composed predominantly of cartilage; 3 when osteophytes were composed of mixed cartilage and bone; and 4 when osteophytes were composed predominantly of bone. Synovitis was scored 0, 1-3 from H&E-stained sections based on the thickness of the synovial cell lining layer and the cell density within this layer [35]. 0 being the thinnest synovial cell lining layer and low cell density (1-2 cell layers), 1 with 3-5 cell layers, 2 with 6-8 cell layers, and 3 being the thickest synovial cell lining layer (>8 layers) and high cell density. Ectopic chondrogenesis was scored 0 when it was undetectable, 1 when it was found in the synovium and or the capsule, and 2 when it extended into the surrounding ligament and or muscle [36].

Immunohistochemistry

At least three sections of the mid coronal region per mouse and an overall 15 samples per sex were used for IHC staining. Following deparaffinization and rehydration, the tissue sections were treated with citrate-based antigen unmasking solution (H-3300, Vector Laboratories, Inc, California, USA). Then endogenous peroxidase activity was inactivated by BLOXALL endogenous blocking solution (SP-6000, Vector Laboratories, Inc, California, USA). After blocking using the protein block solution (ab64226, Abcam, Massachusetts, USA), the sections were incubated overnight with the primary antibodies at 4°C over-night, stained with rabbit specific HRP/DAB(ABC) detection kit (PK-4001/SK-4100, Vector Laboratories, Inc, California, USA) and counterstained by hematoxylin (Sigma, Missouri, USA)). For IHC, primary antibodies were against iNOS (1:300, PA3030A, Invitrogen, Massachusetts, USA), MMP-13 (1:50, 18165-1-AP, Proteintech, Illinois, USA), NLRP3 (1:300, PA5-88709, Invitrogen, Massachusetts, USA), β-galactosidase (1:400; #ab196838, Abcam), and p16 (1:100; #PA30670, Invitrogen). Section images were acquired by DMRXE universal microscope with objective imaging gigapixel montaging workstation (Leica Biosystems, IL, USA) and analyzed using Fiji Image J where positive cells were *manually labeled* to allow automatic counting process (Version 1.5r; NIH, Maryland, USA). Quantification was performed by calculating the percent of positively stained

Poudel *et al. Arthritis Research & Therapy*   (2024) 26:118

Page 5 of 14

cells for respective markers of the total number of chondrocytes confined within 20-μm immediately proximal to femoral condyle and distal to the tibial plateau surface.

Statistical analysis

Individual descriptive statistics (e.g., means, medians, interquartile ranges) were calculated overall and by group for each outcome. The main effects for treatment and sex, as well as the interaction between the two, were estimated using linear regression (for continuous outcomes) and ordered logistic regression (for categorical outcomes). For each pairwise combination of categorical variables, Spearman's rank correlation coefficients were computed overall and within treatment and sex, with adjustment for the family wise error rate using the method of Benjamini and Hochberg [37]. Comparisons between sex-specific correlations within each treatment were made using the Fisher r-to-z transformation. Principal component analyses were conducted for continuous multivariate outcomes by treatment and sex, with any instance of missing data being imputed using the regularized iterative PCA algorithm [38]. Finally, no difference was found in data distribution of samples of the same sex, coming from different centers. The data was normally distributed for each center and there was no difference in the frequency distribution of the different traits between samples from different centers for each sex. Data analysis was conducted in R v4.1.3

Results

Prevalence of primary OA in UM-HET3 mice: assessed the integrity of the AC at the distal femur and proximal tibia (Fig. 1B) and the state of the synovial membrane at the medial and lateral sides of the joint (Fig. 1C). The scores of control male and female mice varied both between and within sexes.

Cumulative AC (cAC) scores across *all the knee joint* (*medial and lateral sides* of *both the tibia and the femur*, that can reach a maximal score of 24) revealed significant difference between male and female mice which developed primary OA to varying degrees (OR 2.15, CI [1.289, 3.609], Fig. 2A,B). However, there was no sex differences within treatment for MB (OR 1.15, CI [0.619, 1.863]) or MitoQ (OR 1.227, CI [0.669, 1.834]).

cAC scores, specifically at the *medial side* of the tibia and the femur (that can reach a maximal score of 12) revealed significant differences between sexes (OR 2.425, CI [1.443, 4.076], Fig. 2C, D). Across all mice, treatment with MB significantly reduced the outcomes (OR 0.429, CI [0.213, 0.866]). On the other hand, MitoQ-treated mice did not show significantly different cAC scores at the medial knee joint (OR 0.903, CI [0.424, 1.924]). In females, 11% of control mice showed no OA with age.

Treatment with MB or MitoQ increased that ratio to 25% and 23%, respectively, with no effect on the proportion of mice scored $1 \leq X \leq 3$ in female mice. Approximately 64% of control females, 67% of MB-treated females, and 69% of MitoQ-treated females exhibited an accumulative score of $4 \leq X \leq 6$ OA.

cAC scores, specifically at the *lateral side* of the tibia and the femur (that can reach a maximal score of 12) revealed no difference between sexes (OR 1.161, CI [0.695, 1.939], Fig. 2E, F). Approximately 66% of control males, 86% of MB-treated males, and 82% of MitoQ-treated males exhibited a cAC score of $1 \leq X \leq 3$ OA in the lateral side. In females, treatment with MitoQ associated with 14% of cAC score of 0 and 87% of cumulative AC score of $1 \leq X \leq 3$. Overall, we found that at the lateral side of the knee joint, treatment significantly differed between sexes. Male mice had 3.575X the odds of female mice of having a high cAC scores (OR 3.575, CI [1.045, 12.226]). Likewise, MitoQ-treated male mice had 3.557X higher odds (OR 3.557, CI [1.539, 20.066]) of having a high cAC score than females.

AC scores correlate with osteophytosis, synovitis and ectopic chondrogenesis

We investigated the relationships between cAC scores (of whole joint; medial and lateral femur and tibia) and three other factors: synovitis (cumulative scores of medial and lateral joint) (Fig. 3A, B), osteophytosis (cumulative scores of medial and lateral joint) (Fig. 3C,D) and ectopic chondrogenesis (Ec.Chond, cumulative scores of medial and lateral joint) (Fig. 3E,F). Score distribution for each of the aforementioned factors was plotted in supplement figure 7. There was no significant difference in the correlation between AC score and synovitis in males versus females (Fig. 3A,B). In the MitoQ group, but not MB, there were significant differences (p=0.0117) in the correlations between cAC and synovitis in males compared to females (Fig. 3G). Notably, we found a significant presence of ossification within the synovial membrane with over 80% of the animals exhibited ectopic chondrogenesis and ossification at the site of the synovial membrane. This ossification greatly affects the precision of evaluating synovial features such as fibrin deposition, vascularization, fibrosis, or perivascular edema, as described in Minten et al [39], which were applied to human samples. Nevertheless, we present synovial membrane sections from both control male and female mice (Supplement Figure 8) to illustrate the vascularization and fibrosis of the synovial membrane.

We used a semiquantitative method to score the degree of osteophytes present in the medial and lateral sides of the knee joint. In male mice, osteophytosis did not correlate with cAC scores (Fig. 3C,D). However, there were
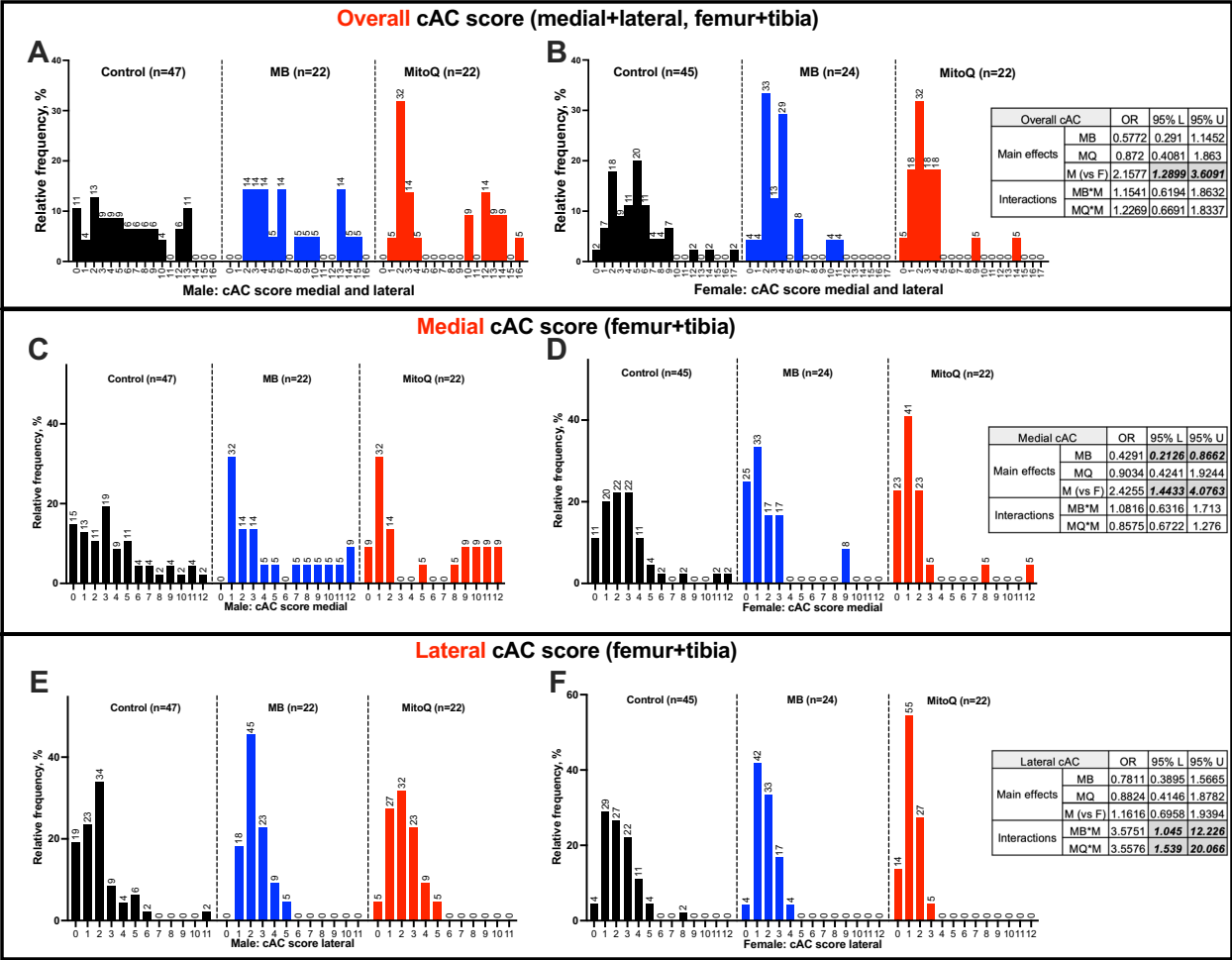
Fig. 2 Prevalence and severity of OA in UM-HET3 mice during aging. The frequency of cAC scores at the medial (**A, B**) and lateral (**C, D**) sides of the knee joints from control (CTL males *n*=47, CTL females *n*=45), MB- (males *n*=22, females *n*=24), and MitoQ-treated (males *n*=22, females *n*=22) mice. The odd ratio (OR) and the coefficient interval 95% upper (U) and lower (L) of the main effects for treatment and sex, as well as the interaction between the two, were estimated using ordered logistic regression, are indicated in the tables

significant differences in the correlations between AC score and ostephytosis in males as compared to females (*p*=0.044) (Fig. 3G). Lastly, there were no correlations between ectopic chondrogenesis and cAC scores in either sex for mice treated with MitoQ or MB (Fig. 3E,F).

AC scores correlate with markers of inflammation in chondrocyte

We used immunohistochemistry (IHC) approach to determine the levels of inflammatory markers in AC chondrocytes of control mice. Three inflammatory markers were selected including MMP-13, iNOS, and the NLRP3 inflammasome. We found significant direct correlations between the AC scores and the protein levels of MMP-13, iNOS, and NLRP3 in chondrocytes at the medial part of the knee joint in both male and female mice (Fig. 4A, supplement figure 1). Similar correlations

were found in the lateral part of the knee joint, although, not all were significant (Fig. 4B). As expected, synovitis score correlated with the protein levels of iNOS, and NLRP3 at the synovial membrane at the medial part of the joint (Fig. 4C, supplement figure 2). Finally, we found significant direct correlations between AC scores and the protein levels of markers of cell cycle arrest including p16 and ß-galactosidase in chondrocytes (supplement figure 3).

SCB morphology in aged UM-HET3 mice was not modified by MB or MitoQ treatment

We examined the morphology of the subchondral bone (SCB) and subchondral plate (SCBP) using micro-CT analysis (Table 1, supplement figure 4). All parameters tested, including SCB volume (bone volume/total volume, BV/TV) in femur (Fig. 5A) or tibia (Fig. 5E),
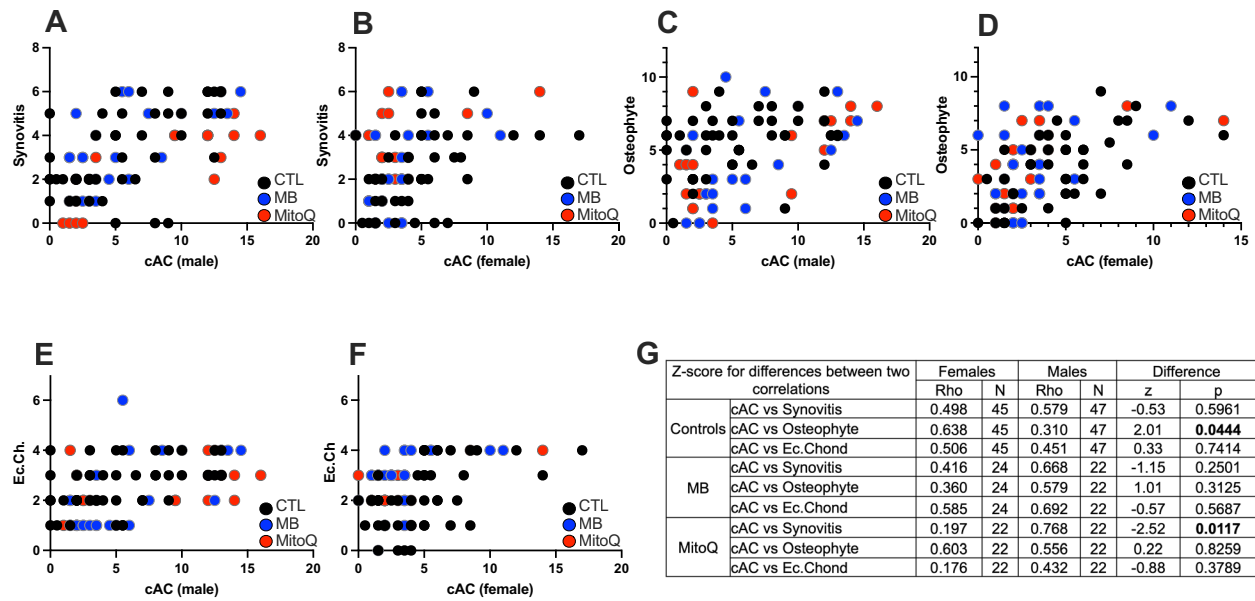
Poudel *et al. Arthritis Research & Therapy*   (2024) 26:118

Page 7 of 14

Fig. 3 Correlations between cumulative AC (cAC) scores and synovitis, osteophytosis, or ectopic chondrogenesis (Ec.Chond). Correlations between cAC scores and synovitis in male (**A**) and female (**B**) mice. Correlations between cAC scores and osteophyte formation in male (**C**) and female (**D**) mice. Correlations between cAC scores and ectopic chondrogenesis in in male (**E**) and female (**F**) mice. A summary table of the Z score differences between each correlation along with the p values (G). CTL males *n*=47, CTL females *n*=45, MB males *n*=22, MB females *n*=24, MitoQ males *n*=22, MitoQ females *n*=22

Z-score for differences between two correlations	Females		Males		Difference	
	Rho	N	Rho	N	z	p
Controls cAC vs Synovitis	0.498	45	0.579	47	-0.53	0.5961
cAC vs Osteophyte	0.638	45	0.310	47	2.01	**0.0444**
cAC vs Ec.Chond	0.506	45	0.451	47	0.33	0.7414
MB cAC vs Synovitis	0.416	24	0.668	22	-1.15	0.2501
cAC vs Osteophyte	0.360	24	0.579	22	1.01	0.3125
cAC vs Ec.Chond	0.585	24	0.692	22	-0.57	0.5687
MitoQ cAC vs Synovitis	0.197	22	0.768	22	-2.52	**0.0117**
cAC vs Osteophyte	0.603	22	0.556	22	0.22	0.8259
cAC vs Ec.Chond	0.176	22	0.432	22	-0.88	0.3789

SCB trabecular thickness (Tb.Th) in femur (Fig. 5B) or tibia (Fig. 5F), or subchondral bone mineral density (BMD) in femur (Fig. 5C) or tibia (Fig. 5G) significantly deferred between sexes but were not altered with treatment. Similarly, tibial SCBP Th (Fig. 5H) or BMD (Fig. 5I), significantly deferred between sexes, and MitoQ treatment significantly increased SCBP BMD (p=0.0438) compared to controls. We found that morphological traits of the SCB in the femur correlated significantly to those of the tibia, indicating that both SCB compartments are regulated in a similar manner (supplement figure 5).

Results from principal component analyses (PCA) suggest that much of the variation in micro-CT measures across samples occurs in two dimensions (70%) (Fig. 5J, K). In both males and females, the strongest influencing measurements included femur SCB BV/TV, femur SCB BMD, and tibia SCB BV/TV for the first component, while femur SCB Tb.Th had substantial influence on the second component. There was a strong positive correlation between femur and tibial measurements with the exception of strong negative correlations with both tibia and femur SCB trabecular spacing (Tb.Sp). Surprisingly, PCA indicate that measurements for the tibia SCBP were largely orthogonal. In males, contributions from tibia SCB Tb.Th and tibia SCBP BMD were not as strong, nor were tibia SCB Tb.Th and tibia SCB Tb.Sp in females. Finally, we did not find significant interactions between SCBP morphology and the cAC scores at the lateral or medial of the tibia (supplement figure 6).

Discussion

OA, a widespread and chronic joint disorder, is marked by ongoing deterioration of cartilage, alterations in subchondral bone, bone marrow lesions, damage to the meniscus, and synovitis. In the current study we utilized 182 stifles of genetically diverse UM-HET3 mice to model the prevalence and severity of primary OA during aging in male and female mice. We found that at the medial side of the knee joint 90% of control female and 85% of control male mice developed primary OA to varying degrees, accompanied by synovitis, osteophytosis, and calcified menisci. Interestingly, 64% of control females showed cAC scores of $1 \leq X \leq 3$, and only 43% of males showed scores at that range in the medial side of the knee joint.

Both male and female control mice showed significant correlations between AC scores and synovitis. In control female mice we found significant correlation between osteophytosis and AC scores. Notably, osteophytes contribute to both the functional properties of affected joints and clinically relevant symptoms. They are closely associated with cartilage damage, although they can also develop without explicit cartilage damage [40]. The precursor cells for osteophyte formation are debatable and include mesenchymal stem cells in the periosteum [41]
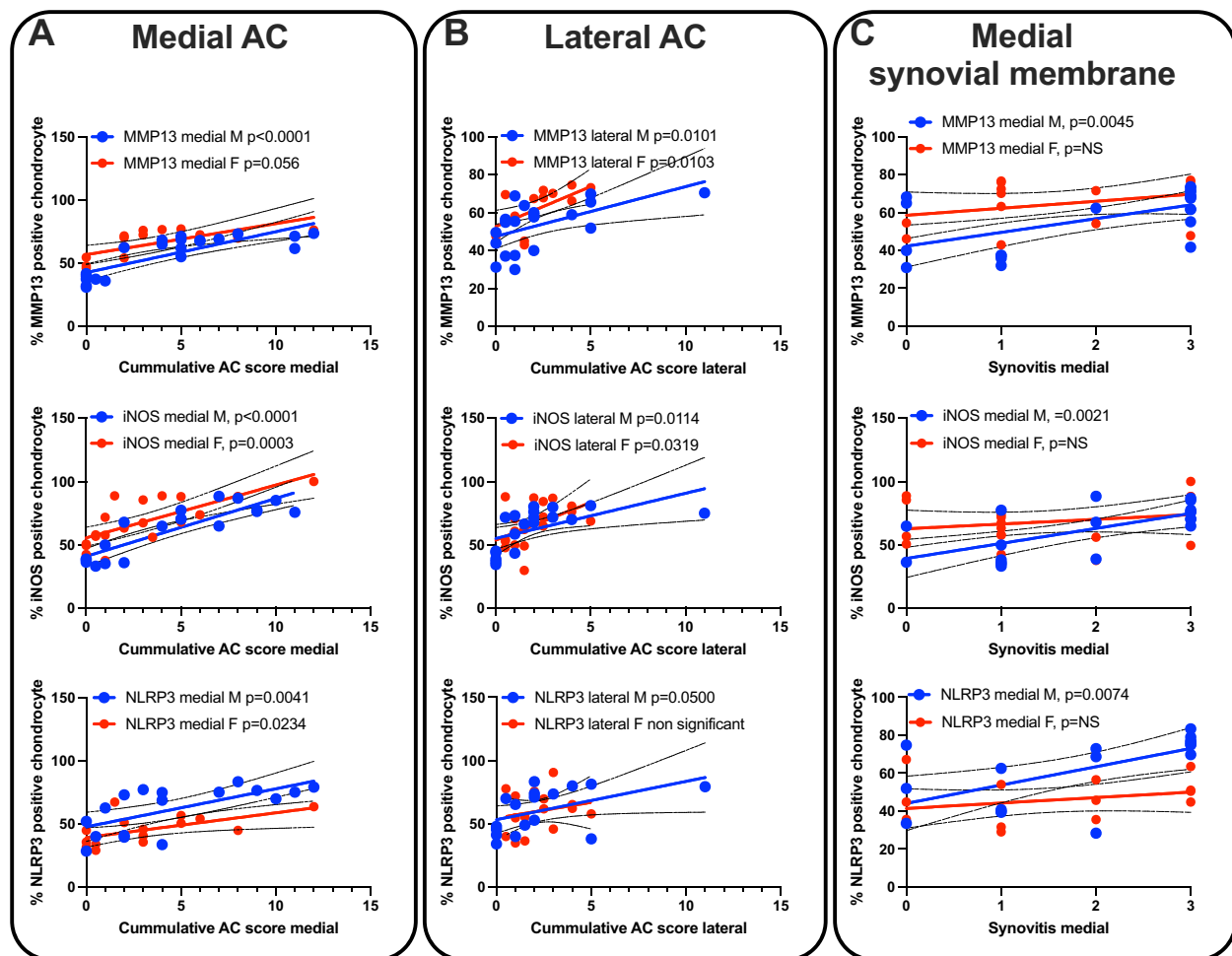
Fig 4 Correlations between cumulative AC scores and markers of inflammation. Correlations between cumulative AC scores at the medial (**A**) and lateral (**B**) side of the joint with the levels of MMP13 (males *n*=21, females *n*=15), iNOS (males *n*=19, females *n*=19), and NLRP3 (males *n*=17, females *n*=15) in AC chondrocytes. (C) Sections of the medial synovial membrane in control mice immunostained with iNOS (males *n*=19, females *n*=19), and NLRP3 (males *n*=17, females *n*=15)

or synovium-derived cells [42]. The TGFβ superfamily of growth factors and macrophages play important roles in osteophyte induction [43]. In control males, osteophytosis did not correlate with AC scores.

The progression of osteoarthritis, triggers inflammatory reaction, characterized by increased expression of the inflammatory markers in AC chondrocytes and cells of the synovial membrane. Specifically, we report significant correlations between protein levels of MMP13, iNOS, and NLRP3 in AC chondrocytes and synovial membrane at the medial knee joint in both male and female mice. Release of inflammatory factors interfere with the anabolic and catabolic activities of chondrocytes and may lead to cell death [44, 45].

Previous studies have reported that mitochondrial dysfunction and oxidative stress contribute to OA development [46]. In chondrocytes, the production

of mitochondrial ROS has been linked to a marked increase in cyclooxygenase, a powerful catabolic inflammatory agent [47] and MMP-13 [48], highlighting their potential role in degradation of the AC. Earlier research has established the significant role of oxidants in modulating metabolic processes in cartilage [49–51]. Together, it is expected that inhibiting excessive ROS accumulation can protect against chondrocyte damages and slow down OA progression. Further, mitochondria in chondrocytes are mechanically connected to the cell membrane through f-actin, facilitating their movement and distribution in the cytosol [52]. This connection between mitochondria and the cytoskeleton plays a crucial role in managing energy and ROS production [50], as well as maintaining calcium balance [53] and controlling mitochondrial apoptotic factors [54]. In light of these evidence, we studied the effects of lifelong

Poudel *et al. Arthritis Research & Therapy*   (2024) 26:118

Page 9 of 14

Table 1 SCB morphology of male and female mice determined by micro-CT. Bone volume/total volume (BV/TV), trabecular thickness (Tb.Th), and bone mineral density (BMD)

		M CTL (n=47)	M MB (n=22)	M MitoQ (n=22)	F CTL (n=45)	F MB (n=24)	F MitoQ (n=22)	Main effects			Interactions	
								MB	MQ	M (vs F)	MB*M	MQ*M
Distal Femur Subchondral Bone												
BV/TV, %	B	21.7618±	20.9130±	21.8811±	17.6319±	17.5472±	17.7906±	-0.526	0.2029	3.924	-0.76258	-0.03787
	SE	0.7489	1.0306	1.5200	0.6837	0.7915	0.9468	1.043	1.0497	0.7396	1.79945	1.85574
	p							0.615	0.847	**3.39E-07**	0.67225	0.983741
Tb.Th, mm	B	0.0688±	0.0678±	0.0687±	0.0749±	0.0759±	0.0789±	-0.000145	0.0019519	-0.0075682	-0.0019332	-0.0041596
	SE	0.0012	0.0020	0.0020	0.0016	0.0022	0.0023	0.00207	0.0020854	0.0014693	0.0035634	0.0036748
	p							0.944	0.351	**6.97E-07**	0.58817	0.25924
Tb.Sp, mm	B	0.2532±	0.2539±	0.2512±	0.3296±	0.3243±	0.3336±	-0.0022881	0.0007131	-0.0762672	0.0060545	-0.0059524
	SE	0.0057	0.0065	0.0109	0.0065	0.0061	0.0096	0.0084013	0.0084558	0.0059576	0.0144828	0.0149359
	p							0.786	0.933	**2.00E-16**	0.676	0.691
Tb.N, 1/mm	B	3.1403±	3.0609±	3.1812±	2.3486±	2.3010±	2.2506±	-0.062927	-0.024334	0.816088	-0.03187	0.138898
	SE	0.0790	0.0990	0.1763	0.0742	0.0653	0.1004	0.110956	0.111676	0.078683	0.191178	0.197159
	p							0.571	0.828	**<2e-16**	0.868	0.482
BMD, g/cc	B	0.2480±	0.2344±	0.2530±	0.2208±	0.2114±	0.2307±	-0.00532	0.001547	0.025015	-0.004436	-0.00509
	SE	0.0072	0.0090	0.0137	0.0072	0.0087	0.0097	0.010117	0.010183	0.007175	0.017461	0.018007
	p							0.599648	0.879432	**0.000619**	0.79975	0.77775
Proximal Tibia Subchondral Bone												
BV/TV, %	B	20.3482±	20.6231±	18.6409±	17.0072±	16.7714±	15.9309±	-1.1174	-0.4082	3.3361	0.46492	-0.67686
	SE	0.6811	1.2275	1.0443	0.7781	1.0041	0.7885	1.0344	1.0038	0.7198	1.76073	1.77353
	p							0.2815	0.6848	**7.09E-06**	0.79207	0.70321
Tb.Th, mm	B	0.0651±	0.0671±	0.0642±	0.0724±	0.0705±	0.0709±	-0.001612	0.0002615	-0.006148	3.83E-03	5.71E-04
	SE	0.0010	0.0015	0.0013	0.0014	0.0018	0.0018	0.0016909	0.001641	0.0011768	2.87E-03	2.89E-03
	p							0.3418	0.8736	**5.06E-07**	0.1828	0.8434
Tb.Sp, mm	B	0.2135±	0.2180±	0.2314±	0.2601±	0.2558±	0.2674±	0.00244	0.010634	-0.041754	0.008938	0.010821
	SE	0.0030	0.0063	0.0057	0.0038	0.0063	0.0056	0.005548	0.005384	0.003861	0.009407	0.009475
	p							0.6607	0.0499	**<2e-16**	0.343	0.255
Tb.N, 1/mm	B	3.1047±	3.0392±	2.8963±	2.3249±	2.3618±	2.2370±	-0.10127	-0.07336	0.72489	-0.10591	-0.12402
	SE	0.0739	0.1355	0.1369	0.0827	0.1231	0.0891	0.11812	0.11463	0.0822	0.20097	0.20244
	p							0.392	0.523	**1.34E-15**	0.599	0.541
BMD, g/cc	B	0.2389±	0.2365±	0.2302±	0.2175±	0.2080±	0.2085±	-0.010901	-0.004595	0.0234	6.80E-03	6.80E-03
	SE	0.0070	0.0105	0.0103	0.0075	0.0105	0.0082	0.01027	0.009966	0.007147	1.75E-02	1.76E-02
	p							0.28999	0.64532	**0.00128**	0.698	0.9957

Table 1 (continued)

|	M CTL (*n*=47)	M MB (*n*=22)	M MitoQ (*n*=22)	F CTL (*n*=45)	F MB (*n*=24)	F MitoQ (*n*=22)		Main effects			Interactions	
								MB	MQ	M (vs F)	MB*M	MQ*M
Tibia Subchondral Plate												
SCB plate Th, mm	0.1080±0.0036	0.0918±0.0055	0.1027±0.0044	0.1009±0.0032	0.0890±0.0061	0.1059±0.0044	B	-0.007202	-0.005887	0.003244	-0.0037615	-0.0097749
							SE	0.004989	0.004816	0.003462	0.0084504	0.008512
							p	0.1507	0.2232	0.3501	0.6568	0.2524
SCB plate BMD, g/cc	0.8638±0.0147	0.8529±0.0168	0.9381±0.0058	0.8914±0.0167	0.8690±0.0190	0.9620±0.0085	B	0.02725	0.03507	-0.02518	0.01436	0.00654
							SE	0.01429	0.01789	0.01727	0.0304	0.03062
							p	0.1295	**0.0438**	**0.0441**	0.6374	0.8312
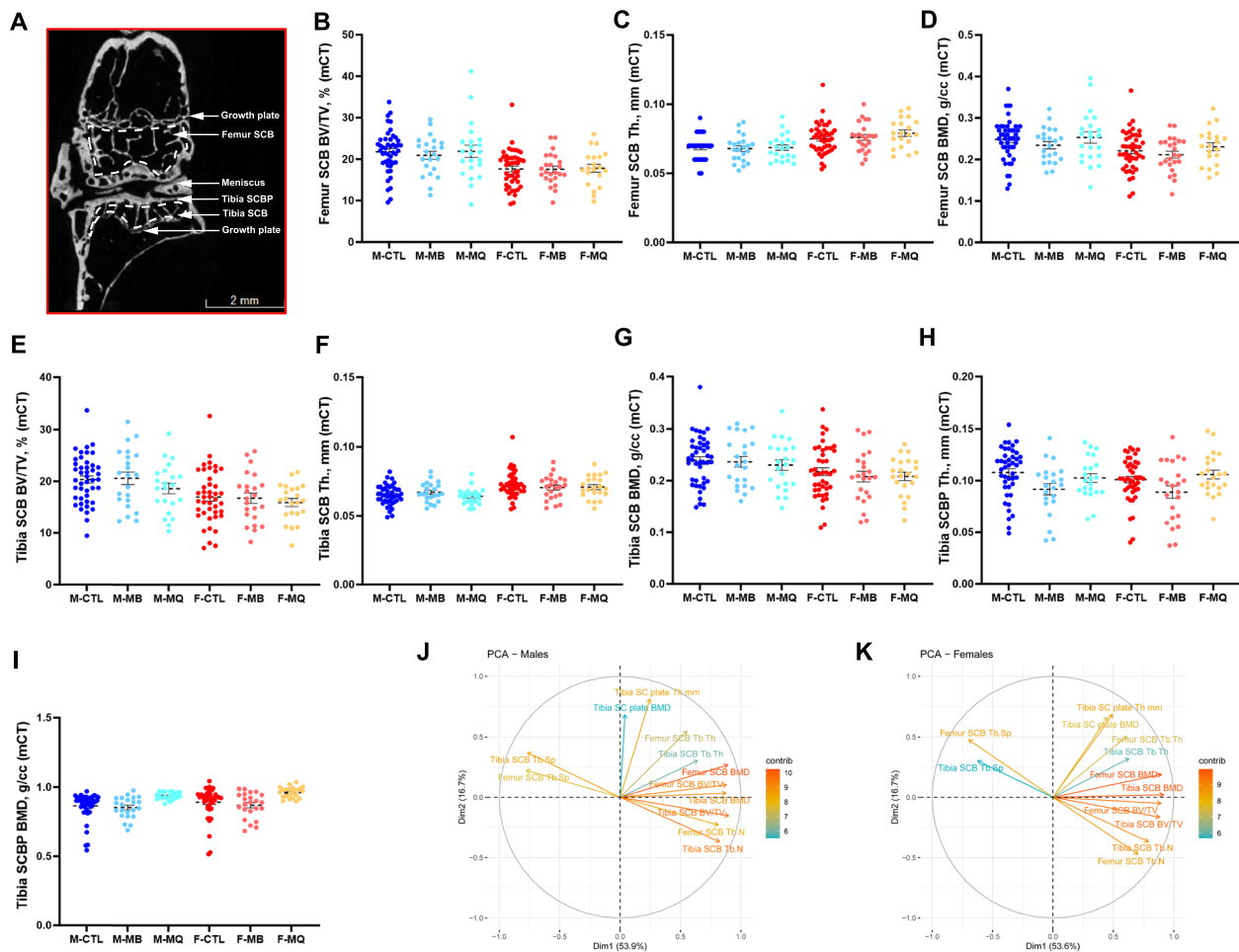
Fig. 5 Subchondral bone (SCB) and subchondral plate (SCP) morphology analyzed by micro-CT. **A** 2D image of a micro-CT scan indicating the knee joint regions of interest that were analyzed including the SCB of the distal femur, SCB of the proximal tibia, and the SCB plate of the proximal tibia. Parameters assessed by micro-CT included femur (**B**) bone volume/total volume (BV/TV), (**C**) trabecular thickness (Tb.Th), and (**D**) SCB mineral density (BMD). Likewise, tibia BV/TV (**E**), Tb.Th of the tibia SCB (**F**), and tibia SCB mineral density (**G**). SCB plate (SCBp) thickness (**H**), and SCBp bone mineral density (**I**), were determined at the proximal tibia. Data presented as mean ± SEM, *p* values are indicated. CTL males *n*=44, CTL females *n*=44, MB males *n*=22, MB females *n*=24, MitoQ males *n*=22, MitoQ females *n*=22. SCB phenotypic measurements from PCA of both male (**J**) and female (**K**) mice. Positively correlated variables point to the same side of the plot; negatively correlated variables point to opposite sides of the plot. Length and color of arrows indicate contribution of the variable to the overall variance of the data. Arrows that are close together are strongly positively correlated, arrows that are about 90 degrees (orthogonal) to each other are uncorrelated, and those far away (such as 180 degrees) are strongly negatively correlated

treatment with MB or MitoQ on the natural history of primary OA in UM-HET3 mice.

MB and MitoQ affect oxidative stress in tissues of the knee joint via different mechanisms. MB ameliorates oxidative stress via stimulation of Nrf2 and its translocation to the nucleus in both in chondrocytes and synoviocytes and exerts anti-inflammatory effects in the synovium and neurons that innervate the knee joint [25]. Evidence from the current study indicate that lifelong treatment with MB lowered the cAC scores compared to controls, suggesting that it may alter the natural history of primary OA in UM-HET3 mice. MitoQ, on the other hand, functions

as a mitochondrial antioxidant [55]. Its lipophilic moiety allows MitoQ to concentrate within mitochondria up to a thousand times more than other general antioxidants [56]. MitoQ is known for its protective effects against diseases related to oxidative damage. In a study using a model of bovine cartilage explants subjected to mechanical stress, MitoQ significantly reduced the production of ROS [30]. Furthermore, MitoQ treatment was found to mitigate the breakdown of the extracellular matrix (ECM), reduce oxidative stress, and lessen the inflammatory response in chondrocytes. This was observed in a mouse model of OA induced by destabilizing the medial

meniscus (DMM) [57] and was likely due to its activation of the NRF2 pathway and the promotion of mitophagy in chondrocytes. In the current study we found that MitoQ-treated male mice had higher lateral, but not medial, cAC scores compared to female mice. Additionally, mice treated with MitoQ, regardless of sex, showed lower measures for SCB Plate BMB in Tibia.

In this study, we report on the prevalence and severity of primary OA in the genetically diverse UM-HET3 mice. We also examined how treating these mice with the antioxidants MB and MitoQ from early adulthood into old age impacts the development of primary OA. Our research has certain limitations, including the fact that we only examined mice at one age range (22-25 months). We established the validity of our model by showing correlations between OA features and indicators of inflammation, synovitis, and osteophyte formation. However, our study did not explore the direct causes of these conditions. We also recognize that our research does not delve into the cellular or molecular mechanisms that might trigger or advance OA. Nevertheless, our findings demonstrate that primary OA in UM-HET3 mice reflects the prevalence and severity seen in human primary OA. This suggests that these mice are a suitable model for testing systemic treatments that could influence aging processes, particularly in the context of developing primary OA.

Conclusions

Our study offers detailed insights into the prevalence and severity of primary OA in aged UM-HET3 mice, mirroring the patterns observed in human primary OA. We demonstrate a link between the degeneration of AC and synovitis, and also uncover sex-specific associations between osteophyte development and AC scores. Additionally, our research sheds light on the impact of MB and MitoQ treatments on primary OA's prevalence and severity. Both treatments reduced the odds ratio (OR) for the onset of primary OA, but only MB showed a significant reduction in the OR in the medial knee joint. Overall, our findings confirm that UM-HET3 mice are an effective model for evaluating systemic treatments aimed at influencing aging processes, especially in relation to the development of primary OA.

Abbreviations

AC	Articular cartilage
BMD	Bone mineral density
BV/TV	Bone volume/total volume
cAC scores	cumulative AC (cAC) scores
CI	Coefficient interval
DMM	Destabilizing the medial meniscus
Ec.Chond	Ectopic chondrogenesis
ECM	Extracellular matrix
IHC	Immunohistochemistry
iNOS	Inducible nitric oxide synthase
ITP	Intervention Testing Program
MB	Methylene blue
MitoQ	Mitoquinone
MMP	Matrix metalloproteinase
Micro-CT	mMicro computed tomography
NIA	National Institute of Aging
NLRP3	NLR family pyrin domain containing-3
OA	Osteoarthritis
OR	Odds ratio
OARSI	Osteoarthritis Research Society International
PCA	Principal component analyses
ROS	Reactive oxygen species
SCB	Subchondral bone
SCBP	Subchondral bone plate
Tb.Th	Trabecular thickness
Tb.N	Trabecular number
Tb.Sp	Trabecular spacing

Supplementary Information

The online version contains supplementary material available at https://doi.org/10.1186/s13075-024-03349-y.

Additional file 1: Supplement Figure 1. Shown are representative knee joint sections stained with MMP-13, iNOS, and NLRP3 antibodies in both male and female mice. Quantification is available in figure 4.

Additional file 2: Supplement Figure 2. Shown are representative medial synovial membrane sections stained with iNOS and NLRP3 in both male and female mice. Quantification is available in figure 4.

Additional file 3: Supplement Figure 3. Shown are representative knee joint sections stained with p16 (A) and quantification of positive chondrocytes in the (B) medial and (C) lateral side of the tibia. (D) Representative knee joint sections stained with b-Gal and quantification of positive chondrocytes in the (E) medial and (F) lateral side of the tibia in both male and female mice. Males n=19 and females *n*=19.

Additional file 4: Supplement Figure 4. (A) 3D images of a micro-CT scan of knee joints from male and female mice with different OA severities (cumulative scores at the medial side of the joint). A link to a short movie presenting 3D reconstruction of knee joints with no histological evidence of OA or with high cumulative AC score obtained by histology (Mendeley Data, V1, doi: 10.17632/6nddwstfw3.1).

Additional file 5: Supplement Figure 5. Femur and tibia SCB traits obtained by micro-CT are significantly directly correlated. Spearman's rank correlations between SCB BV/TV (A,B), SCB BMD (C,D), SCB Th. (E,F), and SCB Tb.N (G,H) of femur and tibia in male and female mice. Males*n*=47, Females *n*=45. *P* values are indicated for each correlation.

Additional file 6: Supplement Figure 6. Cumulative AC (cAC) scores of the medial or lateral tibia show no correlation to the morphology of the SCBP by micro-CT. Spearman's rank correlations between cAC scores at the medial tibia with SCBP Th (A,B) or SCBP BMD (C,D) in male and female mice. Similar correlations were done between cAC scores at the lateral tibia with SCBP Th (E,F) or SCBP BMD (G,H) in male and female mice. Males *n*=47, Females *n*=45. *P* values are indicated for each correlation.

Additional file 7: Supplement Figure 7. A summary of the AC, osteophyte maturity, synovitis, and ectopic chondrogenesis scores at the whole joint, the medial or lateral side of the joint. (A) Cumulative AC (cAC) scores of the whole joint (medial+lateral tibia+femur) in control (CTL) MB-, or MQ-treated male and female mice. (B) cAC scores of the medial joint (medial tibia+femur) in control (CTL) MB-, or MQ-treated male and female mice. (C) cAC scores of the lateral joint (lateral tibia+femur) in control (CTL) MB-, or MQ-treated male and female mice. (D) Cumulative osteophyte maturity scores of the whole joint (medial+lateral tibia+femur) in control (CTL) MB-, or MQ-treated male and female mice. (E) Cumulative osteophyte maturity scores of the medial joint (medial tibia+femur) in control (CTL) MB-, or MQ-treated male and female mice. (F) Cumulative osteophyte maturity scores of the lateral joint (lateral tibia+femur) in control (CTL) MB-, or MQ-treated male and female mice. (G) Cumulative synovitis scores

Poudel *et al. Arthritis Research & Therapy*   (2024) 26:118

Page 13 of 14

of the whole joint (medial+lateral) in control (CTL) MB-, or MQ-treated male and female mice. (H) Synovitis scores at the medial side of the joint in control (CTL) MB-, or MQ-treated male and female mice. (I) Synovitis scores at the lateral side of the joint in control (CTL) MB-, or MQ-treated male and female mice. (J) Cumulative ectopic chondrogenesis (Ect. Chon) scores of the whole joint (medial+lateral) in control (CTL) MB-, or MQ-treated male and female mice. (K) Ect.Chon scores at the medial side of the joint in control (CTL) MB-, or MQ-treated male and female mice. (L) Ect.Chon scores at the lateral side of the joint in control (CTL) MB-, or MQ-treated male and female mice.

Additional file 8: Supplement Figure 8: Representative H&E-stained images of the synovial membrane at the mid-coronal region of the knee joint in both male and female mice. Magnification is at 200X, with scale bars of 150μm and 50μm. A red arrow indicates vascularization, a blue arrow represents fibrosis, and 'OC' denotes ossification in the synovium.

Availability of data and material
Short movies of 3D reconstructed knee joints:Mendeley Data, V1, doi: 10.17632/6nddwstfw3.1 The datasets generated and analyzed during the current study are available upon request. Our studies do not include the use of custom code or mathematical algorithms. We have included citations for available data in the references section.

Declarations

Ethics approval and consent to participate
Animal protocol was reviewed and approved by the Institutional Animal Care and Use Committees of the ITP centers

Consent for publication
NA.

Competing interest
The authors declare no competing interests.

Author details
[1]David B. Kriser Dental Center, Department of Molecular Pathobiology, New York University College of Dentistry, 345 East 24th Street, New York, NY 10010-4086, USA. [2]David B. Kriser Dental Center, Biostatistics Core, Department of Epidemiology and Health Promotion, New York University College of Dentistry, New York, NY 10010-4086, USA. [3]Department of Pathology and Geriatrics Center, University of Michigan, Ann Arbor, MI 48105, USA. [4]The Jackson Laboratory, Bar Harbor, ME 04609, USA. [5]Geriatric Research, Education and Clinical Center and Research Service, South Texas Veterans Health Care System, San Antonio, TX 78229, USA. [6]Barshop Institute for Longevity and Aging Studies and Department of Pharmacology, The University of Texas Health Science Center, San Antonio, TX 78229, USA. [7]Department of Orthopaedic Surgery, NYU Grossman School of Medicine, New York, NY 10100, USA. [8]Department of Biomedical Engineering, NYU Tandon School of Engineering, New York, NY 10010, USA.

References

1. Lotz M, Loeser RF. Effects of aging on articular cartilage homeostasis. Bone. 2012;51(2):241–8.
2. Mobasheri A, et al. Glucose transport and metabolism in chondrocytes: a key to understanding chondrogenesis, skeletal development and cartilage degradation in osteoarthritis. Histol Histopathol. 2002;17(4):1239–67.
3. Salvioli S, et al. Inflamm-aging, cytokines and aging: state of the art, new hypotheses on the role of mitochondria and new perspectives from systems biology. Curr Pharm Des. 2006;12(24):3161–71.
4. Maggio M, et al. Interleukin-6 in aging and chronic disease: a magnificent pathway. J Gerontol A Biol Sci Med Sci. 2006;61(6):575–84.
5. De Martinis M, et al. Inflamm-ageing and lifelong antigenic load as major determinants of ageing rate and longevity. FEBS Lett. 2005;579(10):2035–9.
6. Greene MA, Loeser RF. Aging-related inflammation in osteoarthritis. Osteoarthritis Cartilage. 2015;23(11):1966–71.
7. Ashbrook DG, et al. A platform for experimental precision medicine: The extended BXD mouse family. Cell Syst. 2021;12(3):235-247e9.
8. Saul MC, et al. High-Diversity Mouse Populations for Complex Traits. Trends Genet. 2019;35(7):501–14.
9. Williams RW. Herding cats: the sociology of data integration. Front Neurosci. 2009;3(2):154–6.
10. Miller RA, et al. Preservation of femoral bone thickness in middle age predicts survival in genetically heterogeneous mice. Aging Cell. 2011;10(3):383–91.
11. Reeves GM, et al. Quantitative trait loci modulate vertebral morphology and mechanical properties in a population of 18-month-old genetically heterogeneous mice. Bone. 2007;40(2):433–43.
12. Volkman SK, et al. Quantitative trait loci that modulate femoral mechanical properties in a genetically heterogeneous mouse population. J Bone Miner Res. 2004;19(9):1497–505.
13. Volkman SK, et al. Quantitative trait loci for femoral size and shape in a genetically heterogeneous mouse population. J Bone Miner Res. 2003;18(8):1497–505.
14. Ewart D, et al. Naturally occurring osteoarthritis in male mice with an extended lifespan. Connect Tissue Res. 2020;61(1):95–103.
15. Glasson SS, et al. The OARSI histopathology initiative - recommendations for histological assessments of osteoarthritis in the mouse. Osteoarthritis Cartilage. 2010;18(Suppl 3):S17-23.
16. Kaneko H, et al. Synovial perlecan is required for osteophyte formation in knee osteoarthritis. Matrix Biol. 2013;32(3–4):178–87.
17. Chambers MG, Bayliss MT, Mason RM. Chondrocyte cytokine and growth factor expression in murine osteoarthritis. Osteoarthritis Cartilage. 1997;5(5):301–8.
18. Price JS, et al. The role of chondrocyte senescence in osteoarthritis. Aging Cell. 2002;1(1):57–65.
19. Hui W, et al. Oxidative changes and signalling pathways are pivotal in initiating age-related changes in articular cartilage. Ann Rheum Dis. 2016;75(2):449–58.
20. Loeser RF. Aging and osteoarthritis. Curr Opin Rheumatol. 2011;23(5):492–6.
21. Blanco FJ, Rego I, Ruiz-Romero C. The role of mitochondria in osteoarthritis. Nat Rev Rheumatol. 2011;7(3):161–9.
22. Kan S, et al. Role of Mitochondria in Physiology of Chondrocytes and Diseases of Osteoarthritis and Rheumatoid Arthritis. Cartilage. 2021;13(2_suppl):1102S-1121S.
23. Harrison DE, et al. Acarbose, 17-alpha-estradiol, and nordihydroguaiaretic acid extend mouse lifespan preferentially in males. Aging Cell. 2014;13(2):273–82.
24. Zheng J, Li Q. Methylene blue regulates inflammatory response in osteoarthritis by noncoding long chain RNA CILinc02. J Cell Biochem. 2019;120(3):3331–8.

25. Li JW, et al. Methylene blue prevents osteoarthritis progression and relieves pain in rats via upregulation of Nrf2/PRDX1. Acta Pharmacol Sin. 2022;43(2):417–28.
26. Li X, et al. Methylene blue relieves the development of osteoarthritis by upregulating lncRNA MEG3. Exp Ther Med. 2018;15(4):3856–64.
27. Tauskela JS. MitoQ–a mitochondria-targeted antioxidant. IDrugs. 2007;10(6):399–412.
28. Sanjuan-Pla A, et al. A targeted antioxidant reveals the importance of mitochondrial reactive oxygen species in the hypoxic signaling of HIF-1alpha. FEBS Lett. 2005;579(12):2669–74.
29. Kelso GF, et al. Selective targeting of a redox-active ubiquinone to mitochondria within cells: antioxidant and antiapoptotic properties. J Biol Chem. 2001;276(7):4588–96.
30. Wolff KJ, et al. Mechanical stress and ATP synthesis are coupled by mitochondrial oxidants in articular cartilage. J Orthop Res. 2013;31(2):191–6.
31. Miller RA, et al. An Aging Interventions Testing Program: study design and interim report. Aging Cell. 2007;6(4):565–75.
32. Strong R, et al. Nordihydroguaiaretic acid and aspirin increase lifespan of genetically heterogeneous male mice. Aging Cell. 2008;7(5):641–50.
33. Strong R, et al. Rapamycin-mediated mouse lifespan extension: Late-life dosage regimes with sex-specific effects. Aging Cell. 2020;19(11):e13269.
34. Bouxsein ML, et al. Guidelines for assessment of bone microstructure in rodents using micro-computed tomography. J Bone Miner Res. 2010;25(7):1468–86.
35. Mapp PI, et al. Angiogenesis in two animal models of osteoarthritis. Osteoarthritis Cartilage. 2008;16(1):61–9.
36. Grote CW, M.J.M, Liu X, Lu Q, Wang J. A modified comprehensive grading system for murine knee osteoarthritis: scoring the whole joint as an organ. Osteoarthritis Cartilage. 2022;30(April 2022):S95.
37. Yoav Benjamini YH. Controlling the False Discovery Rate: A Practical and Powerful Approach to Multiple Testing. JR Statist Soc B. 1995;57(1):289–300.
38. Josse J, Husson F. missMDA: A Package for Handling Missing Values in Multivariate Data Analysis. J Stat Software. 2016;70(1):31.
39. Minten MJM, et al. Exploring longitudinal associations of histologically assessed inflammation with symptoms and radiographic damage in knee osteoarthritis: combined results of three prospective cohort studies. Osteoarthritis Cartilage. 2019;27(1):71–9.
40. van der Kraan PM, van den Berg WB. Osteophytes: relevance and biology. Osteoarthritis Cartilage. 2007;15(3):237–44.
41. Shirasawa S, et al. In vitro chondrogenesis of human synovium-derived mesenchymal stem cells: optimal condition and comparison with bone marrow-derived cells. J Cell Biochem. 2006;97(1):84–97.
42. Sakaguchi Y, et al. Comparison of human stem cells derived from various mesenchymal tissues: superiority of synovium as a cell source. Arthritis Rheum. 2005;52(8):2521–9.
43. van Lent PL, et al. Crucial role of synovial lining macrophages in the promotion of transforming growth factor beta-mediated osteophyte formation. Arthritis Rheum. 2004;50(1):103–11.
44. Wang Q, et al. Curcumin attenuates collagen-induced rat arthritis via anti-inflammatory and apoptotic effects. Int Immunopharmacol. 2019;72:292–300.
45. Song J, et al. Dysregulation of the NUDT7-PGAM1 axis is responsible for chondrocyte death during osteoarthritis pathogenesis. Nat Commun. 2018;9(1):3427.
46. Coryell PR, Diekman BO, Loeser RF. Mechanisms and therapeutic implications of cellular senescence in osteoarthritis. Nat Rev Rheumatol. 2021;17(1):47–57.
47. Cillero-Pastor B, et al. Mitochondrial dysfunction activates cyclooxygenase 2 expression in cultured normal human chondrocytes. Arthritis Rheum. 2008;58(8):2409–19.
48. Ahmad R, et al. Involvement of H-Ras and reactive oxygen species in proinflammatory cytokine-induced matrix metalloproteinase-13 expression in human articular chondrocytes. Arch Biochem Biophys. 2011;507(2):350–5.
49. Martin JA, et al. Mitochondrial electron transport and glycolysis are coupled in articular cartilage. Osteoarthritis Cartilage. 2012;20(4):323–9.
50. Sauter E, et al. Cytoskeletal dissolution blocks oxidant release and cell death in injured cartilage. J Orthop Res. 2012;30(4):593–8.
51. Lee RB, Urban JP. Functional replacement of oxygen by other oxidants in articular cartilage. Arthritis Rheum. 2002;46(12):3190–200.
52. Boldogh IR, et al. A protein complex containing Mdm10p, Mdm12p, and Mmm1p links mitochondrial membranes and DNA to the cytoskeleton-based segregation machinery. Mol Biol Cell. 2003;14(11):4618–27.
53. Yi M, Weaver D, Hajnoczky G. Control of mitochondrial motility and distribution by the calcium signal: a homeostatic circuit. J Cell Biol. 2004;167(4):661–72.
54. Gourlay CW, Ayscough KR. The actin cytoskeleton: a key regulator of apoptosis and ageing? Nat Rev Mol Cell Biol. 2005;6(7):583–9.
55. James AM, et al. Interaction of the mitochondria-targeted antioxidant MitoQ with phospholipid bilayers and ubiquinone oxidoreductases. J Biol Chem. 2007;282(20):14708–18.
56. Ng LF, et al. The mitochondria-targeted antioxidant MitoQ extends lifespan and improves healthspan of a transgenic Caenorhabditis elegans model of Alzheimer disease. Free Radic Biol Med. 2014;71:390–401.
57. Hou L, et al. Mitoquinone alleviates osteoarthritis progress by activating the NRF2-Parkin axis. iScience. 2023;26(9):107647.

Publisher's Note